Foss. Rec., 21, 11–32, 2018
https://doi.org/10.5194/fr-21-11-2018

Fossil Record
Open Access
MUSEUM FÜR NATURKUNDE BERLIN

Description of the skeleton of the fossil beaked whale *Messapicetus gregarius*: searching potential proxies for deep-diving abilities

Benjamin Ramassamy[1,2], **Olivier Lambert**[3], **Alberto Collareta**[4,5], **Mario Urbina**[6], **and Giovanni Bianucci**[4]

[1]Natural History Museum of Denmark, University of Copenhagen, Copenhagen, 1350, Denmark
[2]Department of Natural History and Palaeontology, the Museum of Southern Jutland, Gram, 6100, Denmark
[3]D.O. Terre et Histoire de la Vie, Institut royal des Sciences naturelles de Belgique, Brussels, 1000, Belgium
[4]Dipartimento di Scienze della Terra, Università di Pisa, Pisa, 56126, Italy
[5]Dottorato Regionale Pegaso in Scienze della Terra, via Santa Maria 53, Pisa, 56126, Italy
[6]Departemento de Paleontología de Vertebrados, Museo de Historia Natural-Universidad, Lima, 15072, Peru

Correspondence: Benjamin Ramassamy (fbd313@alumni.ku.dk)

Received: 30 July 2017 – Revised: 17 November 2017 – Accepted: 21 November 2017 – Published: 16 January 2018

Abstract. Ziphiidae (beaked whales) are a successful family of medium- to large-sized toothed whales. Their extant members perform regular deep dives beyond the photic zone to forage for cephalopods and fish. Conversely, extinct long-snouted stem ziphiids are interpreted as epipelagic predators. However, some aspects of this hypothesis remain unclear due to the lack of clear morphological proxies for recognizing regular deep divers.

We compared the forelimb, neck, and pterygoid sinus system of the fossil ziphiid *Messapicetus gregarius* with those of other odontocetes to evaluate the potential of these body regions as proxies to assess deep-diving specialization. The reconstructed musculature of the neck and forelimb of *M. gregarius* was also compared with that of other odontocetes. We also quantified variation in the proportions of the forelimb and the hamular fossa of the pterygoid sinus (HF) using 16 linear measurements. The degree of association between diving behaviour in extant odontocetes and these measurements was evaluated with and without phylogenetic correction.

Reconstruction of the neck musculature suggests that *M. gregarius* possessed a neck more flexible than most extant ziphiids due to the lower degree of fusion of the cervical vertebrae and the large insertions for the M. longus colli and Mm. intertransversarii ventrales cervicis. While neck rigidity might be related to deep diving, differences in neck flexibility among extant ziphiids indicate a more complex functional interpretation. The relationship between forelimb morphology and diving behaviour was not significant, both with and without phylogenetic correction, suggesting that it cannot be used to assess deep-diving abilities with the parameters considered here. Measurements of the HF revealed successful to evaluate deep-diving abilities in odontocetes, with an enlargement of this structure in deep divers. Considering other evidence that suggests an epipelagic behaviour, we propose different scenarios to explain the observation of an enlarged HF in *M. gregarius*: (1) this species may have fed at different depths; (2) it performed deep dives to avoid potential predators; or (3) the enlarged HF and deep-diving habitat correspond to an ancestral condition, with *M. gregarius* returning to a more epipelagic habitat.

1 Introduction

Ziphiidae (beaked whales) are a successful family of medium- to large-sized odontocetes (toothed cetaceans) currently represented by at least 22 extant species in 5 genera (Dalebout et al., 2014). The best-known modern ziphiids perform regular dives to reach foraging grounds up to 3000 m, beyond the photic zone, where they capture cephalopods, crustaceans, and bathypelagic fish via suction (Clarke, 1996; Heyning and Mead, 1996; Hooker and Baird, 1999; Johnson et al., 2004; MacLeod et al., 2003; Minamikawa et al., 2007; Schorr et al., 2014; Tyack et al., 2006).

Accordingly, Ziphiidae share a unique set of morphological, physiological, and behavioural adaptations allowing them to optimize the travel time to reach their foraging grounds. First, extant ziphiids travel from the surface in

a vertical position with a slow fluke rate at which the animal is gliding between each fluking period (Tyack et al., 2006). Furthermore, their shortened and fused neck stabilizes their head to maintain a streamlined body during the descent phase (Buchholtz, 2001; Lambert et al., 2013). Likewise, their reduced flipper tucks in an indentation along the body wall to decrease drag forces (Mead et al., 1982). Rommel et al. (2006) have noticed that *Ziphius cavirostris* possesses a flexible rib cage composed of 7 double-headed ribs (vs. 4–5 in *Tursiops truncatus*), 5–6 sternebrae (3–4 in *T. truncatus*), and cartilaginous sternal ribs (composed of bone in *T. truncatus*). The authors have suggested these structures to be related to changes in the thorax anatomy in response to lung collapse during deep dives. Finally, extant ziphiids exhibit an enlarged hamular fossa for the pterygoid sinus (HF), where they store large amounts of air. The pterygoid sinuses are connected to the tympanic cavity. This region around the middle ear bones needs to be surrounded by air to provide acoustic isolation, binaural hearing, and efficient functioning of the ossicular chain (Cranford et al., 2008). At great depth, the large volume of the pterygoid sinuses is thought to be squeezed by the high hydrostatic pressure toward the tympanic cavity, thus permitting ziphiids to hear and use directional echolocation during deep dives (Cranford et al., 2008; Lambert et al., 2013).

Unlike extant beaked whales, some of the long-snouted stem ziphiids (*Messapicetus* spp. and *Ninoziphius platyrostris*) are interpreted as epipelagic predators (Lambert et al., 2015). This hypothesis is based on three arguments. First of all, remains of these species come from platform or coastal deposits, while many fossils of crown ziphiids are recovered in deep-sea deposits (Bianucci et al., 2008, 2013, 2016c; Lambert et al., 2015). Furthermore, the preserved fossil regurgitation of a specimen of *M. gregarius*, composed of numerous epipelagic fish, suggests that this stem ziphiid foraged in shallower grounds than extant ziphiids (Lambert et al., 2015). Finally, stem ziphiids lack some of the morphological adaptations related to suction feeding and deep diving observed in extant species (Lambert et al., 2015). The proportionally longer humerus of *Messapicetus gregarius* suggests that its flipper was longer and thus more subject to drag forces during descent and ascent phases. The lower number or lack of fused cervical vertebrae observed in several adult stem ziphiid specimens indicates a more flexible neck as compared to extant ziphiids. The elongated rostrum of some stem ziphiids bearing numerous functional teeth was less specialized for suction feeding, a feeding strategy often related to deep diving among extant odontocetes (de Muizon, 1984; Lambert et al., 2013, 2015).

Nonetheless, some aspects of this hypothesis remain unclear. Concerning the humerus morphology of *M. gregarius*, only deep-diving extant ziphiids were used for comparison. Including other non-deep-diving odontocetes is necessary to confirm that the elongation of the humerus in *M. gregarius* would impact its diving abilities.

Furthermore, stem ziphiids share with their modern representatives the presence of an enlarged HF and the reduction of the bony lamina laterally limiting the HF (Bianucci et al., 1994, 2010; Lambert et al., 2013). This feature suggests that stem ziphiids were able to hear at great depth, just like modern ziphiids (Lambert et al., 2013). However, proportions of the HF were never quantified in Ziphiidae and compared to other odontocetes.

We have provided here a detailed description of some postcranial remains of the stem ziphiid *Messapicetus gregarius* from the late Miocene (Tortonian) of the southern coast of Peru (Bianucci et al., 2010, 2016b). Then, we have proposed a reconstruction of the musculature of the neck and forelimb for this species and compared it with extant odontocetes with a better-constrained foraging behaviour. Finally, we have quantified variation in the proportions of the forelimb and the HF in odontocetes to identify modifications related to deep-diving specialization.

2 Material and methods

2.1 Specimen preparation

The fossil specimens MUSM 2542 and 2548 were excavated and subsequently transported to the Museo de Historia Natural, Universidad Nacional Mayor de San Marcos, Lima (MUSM). They were prepared and consolidated by means of mechanical tools and standard fossil vertebrate preparation techniques by W. Aguirre under the scientific supervision of R. Varas-Malca in the Departamento de Paleontología de Vertebrados at MUSM.

2.2 Institutional abbreviations

1. IRSNB – Institut Royal des Sciences Naturelles de Belgique, Brussels, Belgium
2. MNHN – Muséum National d'Histoire Naturelle, Paris, France
3. MUSM – Museo de Historia Natural de la Universidad Nacional Mayor de San Marcos, Lima, Peru
4. MSNUP – Museo di Storia Naturale dell'Università di Pisa, Italy
5. NMNZ – National Museum of New Zealand Te Papa Tongarewa, Wellington, New Zealand
6. NRM – Naturhistoriska Riksmuseet, Stockholm, Sweden
7. SNM – Statens Naturhistoriske Museum, Copenhagen, Denmark
8. USNM – National Museum of Natural History, Smithsonian Institution, Washington, DC, USA

Table 1. Set of linear measurements taken on the forelimb and skull of odontocetes.

Measurements	
Hamular fossa of the pterygoid sinus	
1.	Anterior transverse width of the pterygoid sinus (AWP)
2.	Posterior transverse width of the hamular fossa (PWP)
3.	Anteroposterior maximal length of the hamular fossa (LP)
4.	Dorsoventral maximal height of the hamular fossa (HP)
Forelimb (lateral view)	
5.	Maximal scapular length at the right angle (MLS)
6.	Maximal scapula height (MHS)
7.	Glenoid cavity length (GLS)
8.	Anterior-posterior humeral head diameter (AHH)
9.	Maximal length of the humerus (LH)
10.	Maximal distal length of the humerus (DLH)
11.	Width of the humerus at the level of the deltoid tuberosity (WDTH)
12.	Maximal length of the radius (LR)
13.	Width at mid-length of the radius (MLR)
14.	Proximal width of the radius (PWR)
15.	Distal width of the radius (DWR)

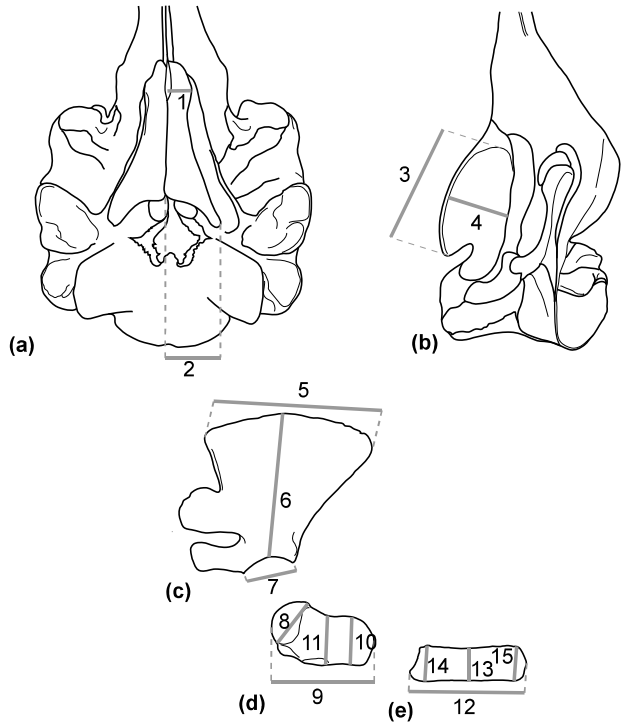

Figure 1. Set of linear measurements taken for the study exemplified in *Hyperoodon ampullatus*. **(a)** Skull in ventral view; **(b)** skull in lateral view; **(c)** scapula in lateral view; **(d)** humerus in lateral view; **(e)** radius in lateral view.

2.3 Terminology

The terminology used by Marx et al. (2016) and Fitzgerald (2016) was followed to describe the postcranial remains of *Messapicetus gregarius*. Muscle origins and insertions follow the nomenclature of the Standard Nomina Veterina Anatomica (International Committee on Veterinary Gross Anatomical Nomenclature, 2005). Muscle development was estimated using osteological markers found on postcranial remains of *M. gregarius* based on previous studies of cetacean myology (Benke, 1993; Cooper et al., 2007; Marx et al., 2016; Sanchez and Berta, 2010; Schulte, 1916; Uhen, 2004). These studies were used for the comparative work with the addition of direct observations from specimens of different institutions (see Dataset 1, (Ramassamy et al., 2018) for the complete list of specimens). The terminology used by Fraser and Purves (1960) was followed to discuss aspects of the pterygoid sinus morphology.

2.4 Statistical analyses

A set of 11 linear measurements for the forelimb and 4 linear measurements for the HF of odontocetes were selected with regard to the preserved parts of *Messapicetus gregarius* and directly measured with digital calipers (0.1 mm) to quantify the morphological variation (Table 1 and Fig. 1). Measurements of the HF and the forelimb were analysed separately. The dataset with HF measurements contained 48 specimens, while the dataset with forelimb measurements contained 46 specimens, each from 27 species (see Dataset 2, Ramassamy et al., 2018).

Two separate methods were applied to correct for intraspecific variation related to ontogenetic development. In the case of forelimb measurements, the method of the log-shape ratios was used (Mosimann, 1970). A variable "size" was computed as the geometric mean of all measurements of a particular structure for each individual. Each measurement for each specimen was then divided by the variable size. Finally, log transformation was performed on each divided measurement. The log-shape ratio procedure removes the effect of size, a variable that is interesting in the case of the HF. To keep the effect of size, raw measurements of the HF were analysed after applying a natural logarithmic transformation (Marcus, 1990). For each dataset, the median of the corrected values was computed for each sampled species and was used for the next analyses.

Phylogenetic comparative methods were required to evaluate the degree of association between deep-diving abilities and proportions of the forelimb and HF due to the disparity of odontocete species compared. Indeed, measurements from closely related species are statistically non-independent, thus precluding the use of statistical methods before correction (Felsenstein, 1985).

The topology of the subtree and divergence time used in this analysis were taken from the cetacean tree by McGowen et al. (2009), including all extant species sampled in this

study. Up to now, no phylogenetic analysis includes the fossil species *Messapicetus gregarius* with all other extant odontocetes of our sample. Therefore, *M. gregarius* was simply added at the base of the ziphiid clade from McGowen et al. (2009). This relationship is supported by the most recent cladistic analyses including fossil Ziphiidae (Lambert et al., 2013; Bianucci et al., 2016a).

A phylogenetic principal component analysis (pPCA; Revell, 2009) was performed to visualize the results for the measurements of the forelimb and the HF of odontocetes with regard to their specialization for deep diving. The pPCA is an exploratory tool similar to the principal component analysis (PCA). The latter is used to reduce the dimensions of a multivariate set of observations, allowing for a discussion of the pattern of variation in the dataset. The original data are translated in a new coordinate system centred toward the mean of the different traits of the dataset and where the rotated axes correspond to the major axes of variation. The PCA conserves the variance and thus the distances between observations. Unlike a conventional PCA, the pPCA takes into account the topology of the tree by centring the dataset toward the estimated phenotype of the root node of the tree instead of the mean and by inversely weighting the covariance matrix by the phylogeny. Consequently, the major axes do not maximize variation, but represent the non-phylogenetic residual variation (Revell, 2009).

A Q-mode for phylogenetic regression method (D-PGLS) was used to control for the phylogenetic independence of the measurement residuals (Adams, 2014). A Brownian motion model of evolution was assumed. The D-PGLS is an extension of the phylogenetic generalized least squares (PGLS). The PGLS is a statistical method aiming at estimating the parameters of a linear regression between two variables while removing the effect of kinships (Martins and Hansen, 1997). The covariance due to the phylogeny is incorporated into the residual error, thus making them statistically independent. The main problem with the PGLS is that it can only accommodate one dependent variable, while our dataset contained multiple measurements. The D-PGLS is a distance-based method using a matrix of pairwise distances among specimens instead of the variance–covariance matrices used in the traditional PGLS (Adams, 2014). This method bears the advantage of accommodating multiple dependent variables, no matter the number of trait dimensions.

Multilinear linear models without phylogenetic correction were also performed using a multivariate analysis of variance (MANOVA) to see if the results differed from the D-PGLS.

While the measurements were the dependent variables, deep-diving specialization was chosen as the categorical explanatory variable. An arbitrary criterion was chosen to assess deep-diving species based on records of the deepest foraging dives for each species. Species were considered specialized deep divers when their deepest foraging dives recorded were 700 m or beyond. Deepest foraging dive depths for each species were collected from the literature (see Dataset 3, Ramassamy et al., 2018). Deepest foraging dives rather than mean foraging dives were selected for two reasons. First, quantitative data were not accessible for all species. Second, deepest foraging dives were assumed to better reflect maximal diving performances for each species, which would be limited by morphological or physiological factors, such as the HF size.

No depth records were found for *Cephalorhynchus commersonii, Platanista gangetica, Sotalia fluviatilis*, *Mesoplodon bidens*, *M. bowdoini*, and *M. grayi*. *C. commersonii*, *P. gangetica*, and *S. fluviatilis* were considered as non-deep divers because these species live in riverine systems or coastal waters (see Dataset 3, Ramassamy et al., 2018). Species of the genus *Mesoplodon* were all considered as deep divers based on *M. densirostris*, for which several diving records are known, and indirect evidence for other species (feeding areas and prey types; e.g., McLeod et al., 2003; Mead, 1989).

The extinct *Messapicetus gregarius* was not considered in the D-PGLS because its diving abilities are based on indirect evidence (Lambert et al., 2015). The basilosaurid *Dorudon atrox* was included in the analysis to evaluate whether the characteristics observed in Ziphiidae were a derived condition or symplesiomorphic. Averages from the measurements of the forelimb of *D. atrox* were taken from Uhen (2004). In agreement with the paleoenvironmental habits of *D. atrox* as reconstructed by Uhen (2004), this species was not considered as a deep diver in the present analysis.

All statistical analyses were performed with the software R 3.2.2 (R Development Core Team, 2015) with the packages car (Fox and Weisberg, 2011), geomorph (Adams and Otarola-Castillo, 2013), phytools (Revell, 2012), and caper (Orme, 2013). The script is available in Dataset 1 (Ramassamy et al., 2018).

3 Systematic Paleontology

Order **Cetacea** Brisson, 1762

Suborder **Odontoceti** Flower, 1867

Family **Ziphiidae** Gray, 1850

Genus *Messapicetus* Bianucci, Landini and Varola, 1992

Messapicetus gregarius Bianucci, Lambert and Post, 2011

3.1 Referred material

Specimen MUSM 2548: three cervical vertebrae including the axis, three thoracic and two thoracic–post-thoracic vertebrae all lacking the neural spine (Figs. 2–3), fused manubrium and left part of the second sternebra (Fig. 4), 11 complete to subcomplete ribs (Fig. 5); skull and mandibles are still in the field. Specimen MUSM 2542: partial right

scapula lacking the acromion, the anterior part of the scapular blade, and the broken coracoid process (Fig. 6); partial left and right humeri (Fig. 7), complete left radius (Fig. 8); skull, mandibles, and other vertebrae of this individual are still in the field.

3.2 Horizon and locality

The specimens were discovered in the 200 m thick section of sediments from the Pisco Formation exposed at Cerro Colorado. They were identified under the fieldwork numbers O37 and O39 in the map provided by Bianucci et al. (2016b).

Two depositional sequences of the Pisco Formation, P1 and P2, are represented at Cerro Colorado and separated by an angular unconformity (Di Celma et al., 2016, 2017). The specimens MUSM 2542 and MUSM 2548 originate from the P1 sequence (the "lower allomember" of Di Celma et al., 2016), consisting of nearshore conglomerates and fine-grained sandstones, bioturbated sandy siltstones, and mudstones (Di Celma et al., 2016). The lower allomember is rich in marine fossil vertebrates, such as cartilaginous and bony fish, marine turtles, crocodiles, sea turtles, sea birds, and seals (Bianucci et al., 2016b; Landini et al., 2017a, b; Parham and Pyenson, 2010; Stucchi et al., 2016). Cetaceans are represented by diverse taxa: Physeteroidea (*Livyatan melvillei* and aff. *Acrophyseter* sp.), Ziphiidae (*M. gregarius*, *Chimuziphius coloradensis*), Inioidea (*Brachydelphis mazeasi* and an undescribed taxon), two undescribed kentriodontid-like Delphinida, Balaenopteroidea, and Cetotheriidae (Bianucci et al., 2010, 2016b, c; Collareta et al., 2015; Gioncada et al., 2016; Lambert et al., 2010a). The geological age of the lower allomember is estimated as 9.9–8.9 Ma (Tortonian, Late Miocene) based on the presence of the diatom species *Lithodesmium reynoldsii* and radiometric dating of a local ash layer (Di Celma et al., 2016; Gariboldi et al., 2017). Diatom genera found in the lower and upper allomembers (e.g., *Delphineis*, *Odontella*, *Rhaphoneis*, *Diplomenora*) are typical of a neritic environment, whereas open-ocean diatoms species are less frequent (Di Celma et al., 2016; Gariboldi et al., 2017).

3.3 Systematic attribution

Both specimens were identified based on complete skulls and mandibles that were left on the field. They are attributed to the family Ziphiidae based on the enlargement of the hamular fossa of the pterygoid. In MUSM 2548, this is further confirmed by the presence of an enlarged apical alveolus on the mandible. The two skulls have an extremely elongated rostrum, representing approximately 75 % of the total condylobasal length. Furthermore, MUSM 2548 displays the medial fusion of the premaxillae dorsal to the mesorostral groove along the rostrum. These two characteristics are typical of the genus *Messapicetus*.

The species *M. gregarius* is by far the most common ziphiid species in the lower allomember of Cerro Colorado, being represented by at least 13 specimens (Bianucci et al., 2016b, c).

4 Results

4.1 Description

4.1.1 Overview and ontogeny

Both specimens are interpreted as adults based on the fully fused epiphyses of the vertebrae of MUSM 2548, the humeral head fused to the humeral shaft, and the epiphyseal ankylosis of each epiphysis of the radius in MUSM 2542. In the small odontocete *Phocoena phocoena*, extensive ankylosis of the postcranial skeleton characterizes adult specimens (Galatius and Kinze, 2003).

4.1.2 Axial skeleton

Axis. The subcomplete axis from specimen MUSM 2548 lacks the left lower transverse process, the left upper part of the neural canal, and the neural spine (Fig. 2a–c). The articulation facet with C3 is transversely wider than dorsoventrally high, with a height of 55 mm and a width of 76 mm. The neural canal was originally oval, transversely wider than dorsoventrally high. The odontoid process is developed anteriorly, but not transversely widened, indicative of a small contact surface with the atlas. The well-developed lower transverse process (75 mm) is oriented lateroventrally. Its posterior surface is excavated along most of its surface. Two fossae medially separated by the hypapophysis excavate the ventral surface of the centrum of the axis.

Other cervical vertebrae. The two other preserved cervical vertebrae from specimen MUSM 2548 are subcomplete and identified as putative C5–C6 (Fig. 2d–f) and C7 (Fig. 2g–i).

One cervical vertebra is referred to as C5 or C6 based on the presence of a vertebrarterial canal extended along the whole dorsoventral height of the centrum, the presence of a lower transverse process measuring 29 mm transversely, and the anterior and posterior articular facets dorsoventrally smaller than transversely wide. These features were observed in C5 and C6 of several extant ziphiid species (*Berardius arnuxii*, *Mesoplodon bidens*, *M. bowdoini*, *M. densirostris*, and *M. grayi*; see Dataset 1 (Ramassamy et al., 2018) for the institution numbers). The neural canal shape is estimated as pentagonal based on the preserved part of the dorsolaterally directed left pedicle (Fig. 2d). The other cervical vertebra is identified as C7 based on the centrum being more dorsoventrally compressed than in C5–C6 and the presence of a fovea for the first rib capitulum on the lateral surface of the vertebra. Lower transverse processes are absent along the vertebra centrum.

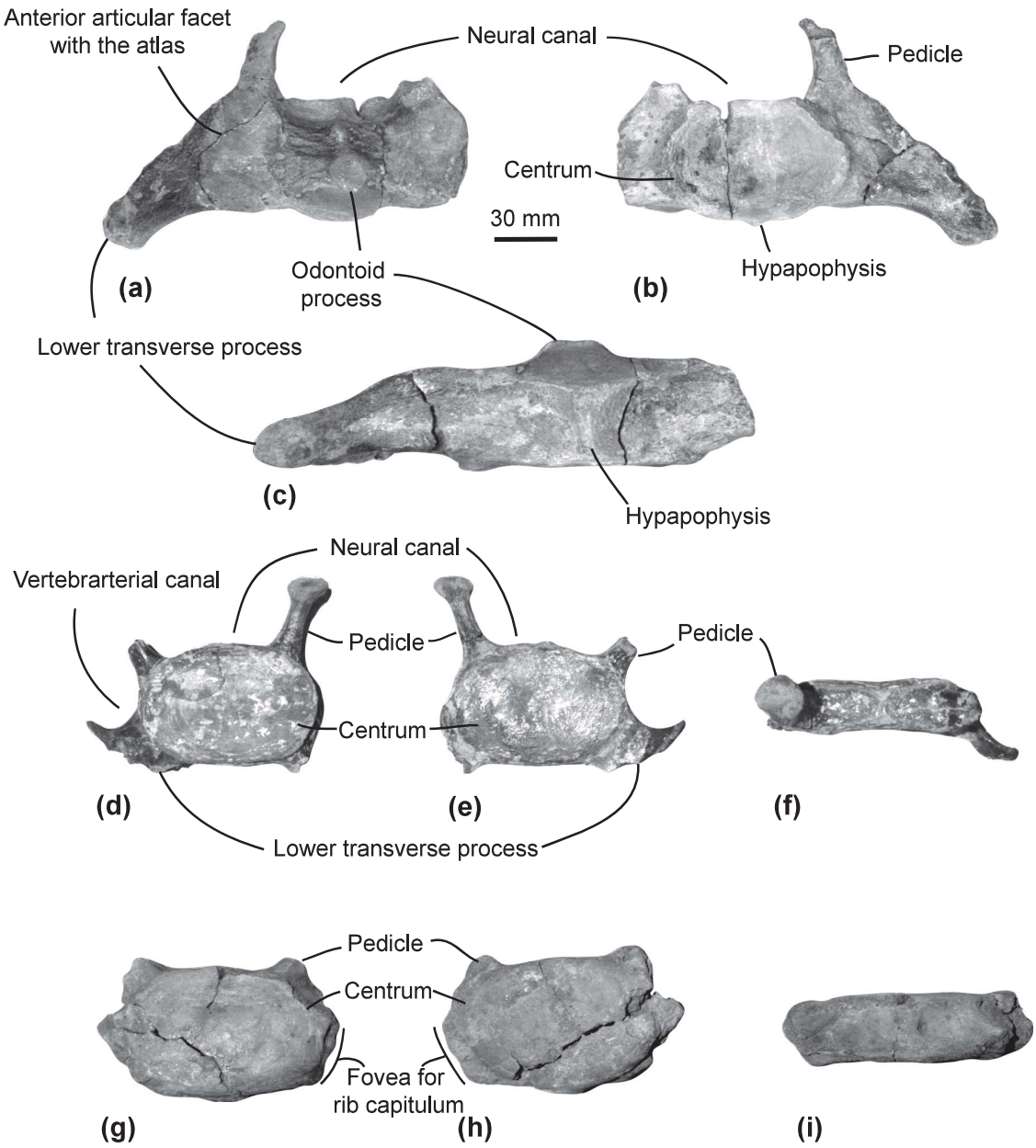

Figure 2. Cervical vertebrae of the specimen MUSM 2548, *Messapicetus gregarius*. Axis in anterior **(a)**, posterior **(b)**, and ventral view **(c)**; C5–C6 in anterior **(d)**, posterior **(e)**, and dorsal view **(f)**; C7 in anterior **(g)**, posterior **(h)**, and dorsal view **(i)**.

Thoracic–post-thoracic vertebrae. The specimen MUSM 2548 is represented by three thoracic and two thoracic–post-thoracic vertebrae (Fig. 3). Their precise position along the vertebral column cannot be identified in the absence of the complete series. Consequently, a relative position is given here in an anteroposterior sequence from A to E.

All thoracic and post-thoracic vertebrae possess a centrum transversely wider than dorsoventrally high (Table 2) and oval in shape. An exception to this pattern is the anterior epiphysis of vertebra A, which is dorsoventrally higher than transversely wide and more rectangular (Fig. 3a). Vertebrae A, B, and G are identified as thoracics because of the presence of a fovea for the rib tuberculum on the upper transverse process and a fovea for the rib capitulum along their centrum (Fig. 3a–b and 3d). In posterior view of vertebrae A, B, and G, the fovea for the rib capitulum is located along the dorsolateral surface of the centrum. The extent of this fovea suggests these to be posterior to the thoracic vertebra 1. Indeed, in all extant Ziphiidae examined, the fovea extends along the whole lateral surface of the centrum.

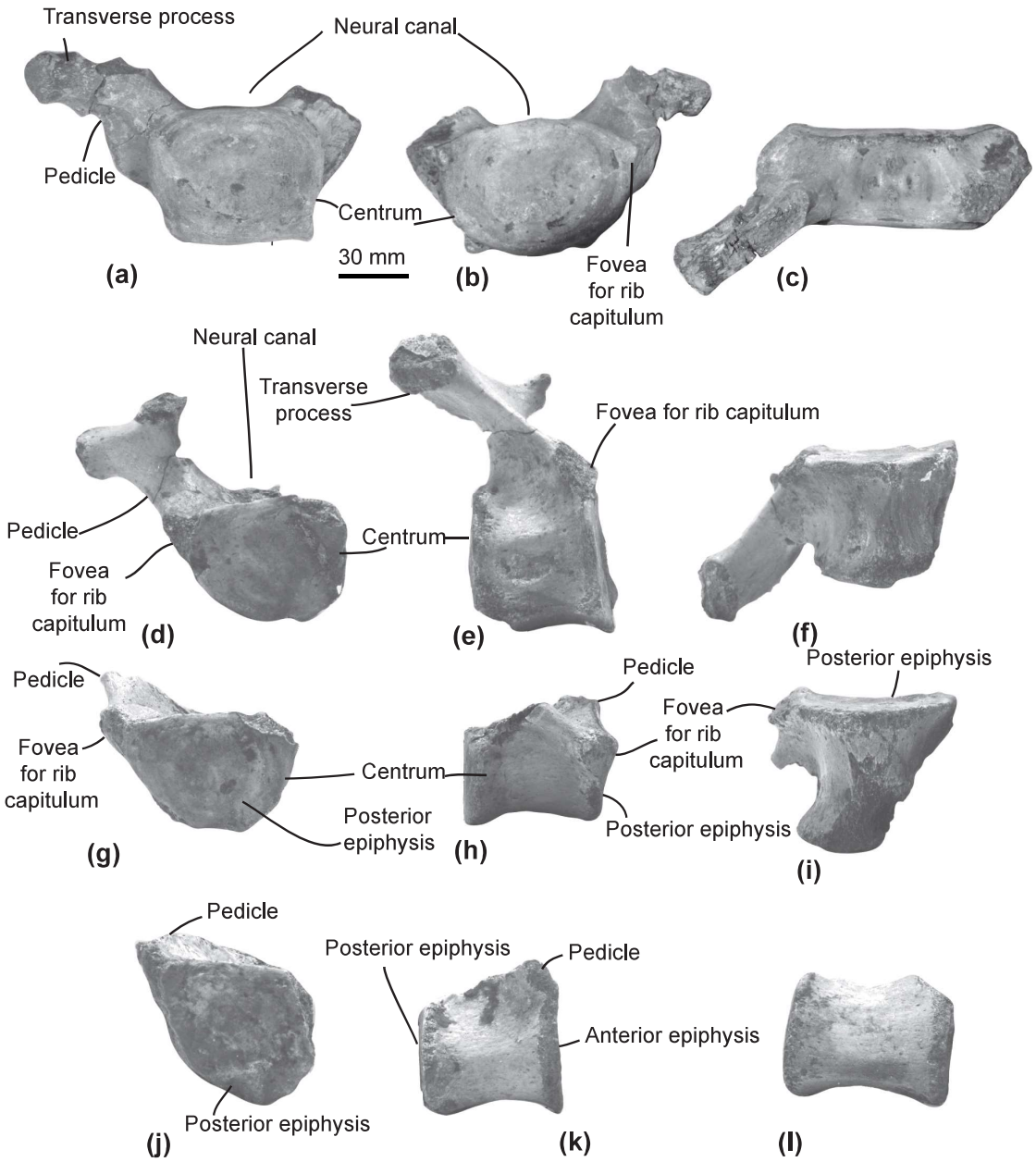

Figure 3. Thoracic and post-thoracic vertebrae of the specimen MUSM 2548, *Messapicetus gregarius*. Thoracic vertebra A in anterior **(a)**, posterior **(b)**, and dorsal view **(c)**; thoracic B in posterior **(d)**, left lateral **(e)**, and ventral view **(f)**; thoracic C in posterior **(g)**, lateral **(h)**, and ventral view **(i)**; thoracic–post-thoracic D in posterior **(j)** and lateral view **(k)**; thoracic–post-thoracic E in lateral view **(l)**.

4.1.3 Sternum and ribs

Sternum. Two elements of the sternum are preserved in the specimen MUSM 2548: the complete manubrium and the left half of the sternebra 2 (Fig. 4). The two elements are unfused to each other. The manubrium is roughly H-shaped, its anterior margin being marked by a jugular notch. This bone is transversely wider (at least 220 mm) than anteroposteriorly long (193 mm). In anterior view, it is ventrally convex (Fig. 4b). Its lateral margin is concave, progressively narrowing posteriorly. A medial notch is present posteriorly, longer anteroposteriorly than transversely wide. The two posteriormost margins of the manubrium are less transversely widened than the anteriormost margins. An articular facet for the first rib is present anterolaterally. The shape of the preserved left element of sternebra 2 is similar to the left

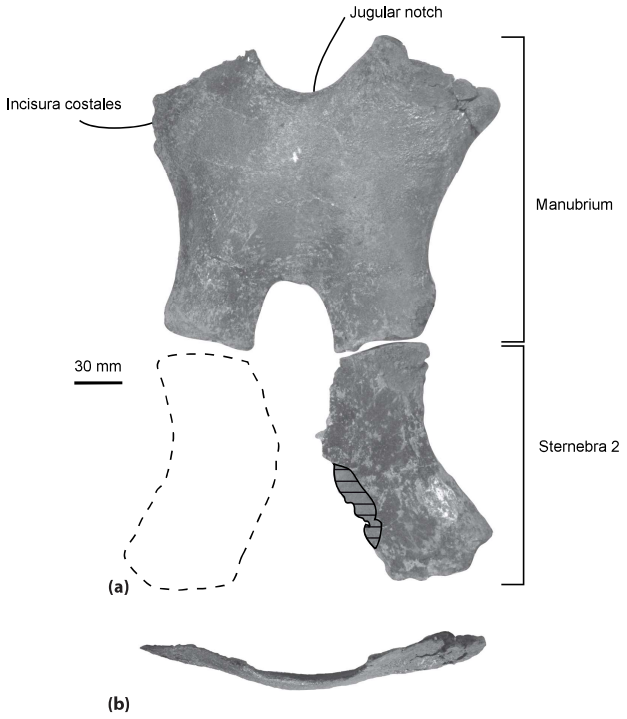

Figure 4. Sternum of the specimen MUSM 2548, *Messapicetus gregarius*, in ventral view (**a**) and manubrium element in anterior view (**b**). Horizontal solid lines indicate major break. The dashed line represents a reconstruction of the second element of the sternebra 2.

half of the manubrium, except for the deeper excavation of its lateral margin.

Ribs. Among the 12 partial ribs recovered in specimen MUSM 2548 (Fig. 5), four pairs are tentatively positioned based on respective head shape (Fig. 5a–h) and by comparison with the identified ribs of *Ninoziphius platyrostris* (de Muizon, 1984). The first pair (Fig. 5a–b) is the shortest. Compared to the other ribs, it possesses the shortest neck, the widest and flattest body, and the thickest angle. The following pairs until pair 4 are progressively longer, thinner, and less flattened, with a longer neck and a shorter capitulum. At least the four first pairs are double-headed. The distal part of each rib is flattened and exhibits longitudinal striations, most likely where muscles inserted.

4.1.4 Forelimb

Scapula. The fan-shaped partial right scapula of MUSM 2542 is marked by multiple fractures. Some pieces were displaced, thus slightly affecting its original shape (Fig. 6). In ventral view, the glenoid cavity is oval and more elongated anteroposteriorly than transversely wide. Posterodorsally to the glenoid fossa, the base of the coracoid process is too damaged to allow for a reconstruction. In lateral view, on the posterior surface of the scapula, a crest separating the infraspinous fossa from the teres fossa is salient dorsoventrally.

Humerus. The two humeri of the specimen MUSM 2542 are partially preserved. Since the left humerus lacks the humeral head and is less well preserved (Fig. 7e–i), only the right humerus is described here (Fig. 7a–d).

The shaft of the right humerus is broken at mid-length, slightly displacing dorsally the distal articulation with the radius and the ulna (Fig. 7a–d). The humeral head is hemispherical and separated from the great tuberosity by a neck visible in ulnar and radial view (Fig. 7c–d). In lateral view, the head of the humerus represents one-third of the total length of the humerus (Fig. 7b). In medial view, the surface of the great tuberosity is flattened, approximately reaching the same proximal level as the head of the humerus. In lateral view, a deltoid ridge is developed along the anterior margin of the humerus at approximately mid-length of the humerus.

In distal view, the articular facets for the radius and the ulna are separated by the distal crest. In lateral view, each articular facet occupies approximately half of the distal surface of the humerus.

Radius. The left radius of MUSM 2542 is complete (Fig. 7j–l). It curves proximodistally and slightly transversely. The facet for articulation of the humerus is oriented anteroproximally. Distally, the articulations for the scaphoid and the lunate can be differentiated based on their orientation (Fig. 7j–k). Each occupies approximately half of the distal anteroposterior width of the radius. The articulation for the scaphoid appears straight in lateral view, distally facing, while the articulation for the lunate is more oblique, posterodistally facing.

4.2 Muscle reconstruction of *M. gregarius* and comparisons with other ziphiid species

4.2.1 Neck muscles

M. longus colli. In extant cetaceans, this muscle originates from the lower transverse process of C6 (Schulte, 1916; Uhen, 2004). It inserts into the ventral surface of the axis centrum. The M. longus colli flexes the neck. The origin of the M. longus colli could not be reconstructed here because of the uncertainty of the putative C5–C6 identification. In *Messapicetus gregarius*, right and left muscles inserted into the ventral excavations of the axis centrum separated by the hypapophysis (Fig. 8a).

The axis of *Ninoziphius platyrostris* displays ventral excavations for the M. longus colli similar to *M. gregarius*. Furthermore, de Muizon (1984) interpreted the presence of a ventral tubercle located on the atlas as another region of insertion for the M. longus colli. The M. longus colli most likely originated from the lower transverse process of C6 of *N. platyrostris*, even though we could not identify the precise area. Transversely, the preserved lower process of C6 in *N. platyrostris* measured 20 mm long. It was similar in size and shape to the lower transverse process of the putative C5–C6 of MUSM 2548.

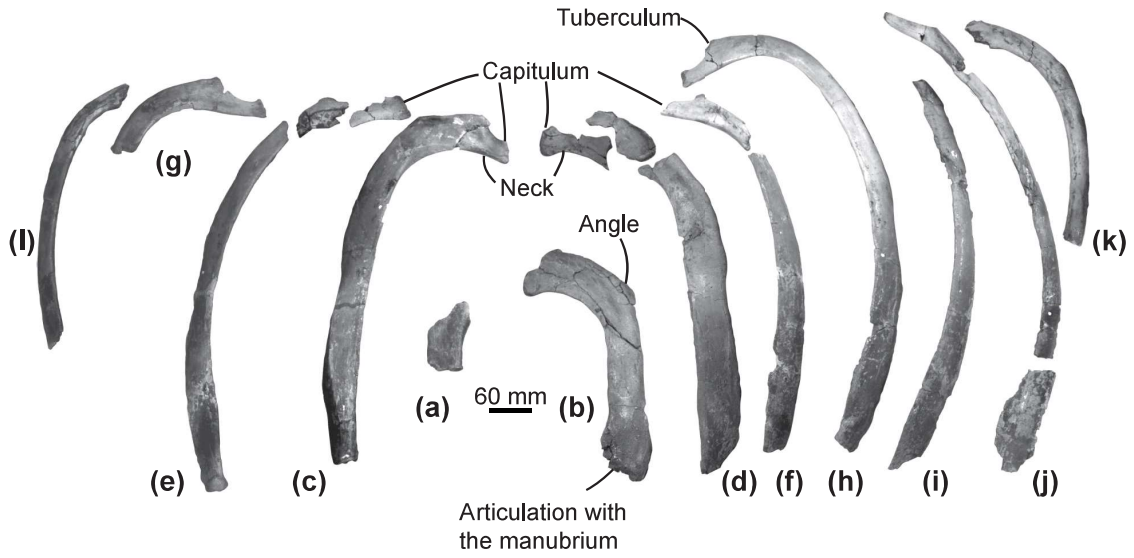

Figure 5. Ribs of the specimen MUSM 2548, *Messapicetus gregarius*, in anterior view. Pair 1 **(a)** and **(b)**; pair 2 **(c)** and **(d)**; pair 3 **(e)** and **(f)**; pair 4 **(g)** and **(h)**; **(i)**, **(j)**, **(k)**, and **(l)** cannot be precisely positioned.

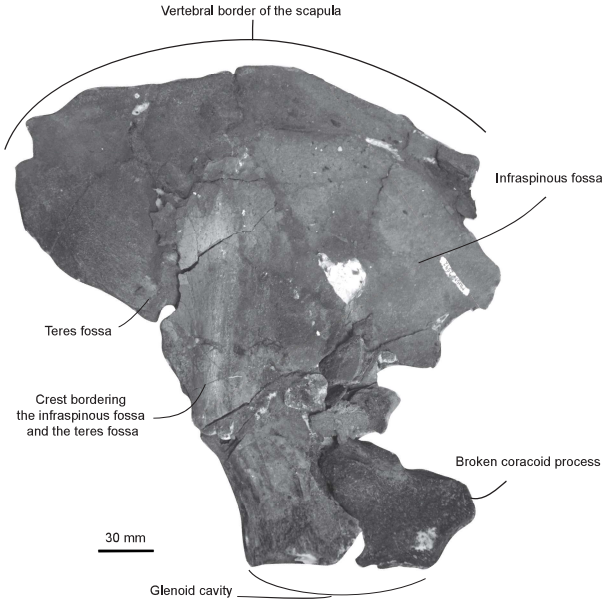

Figure 6. Right scapula of the specimen MUSM 2542, *Messapicetus gregarius*, in dorsal view.

Heavily abraded posteroventrally, the partial atlas of the middle Miocene Berardiinae *Archaeoziphius microglenoideus* probably had a poorly developed (if any) ventral tubercle (Lambert and Louwye, 2006). This suggests a reduction of the M. longus colli insertion area as compared to *N. platyrostris*. The atlas of the late Miocene crown ziphiid *Nazcacetus urbinai* lacks a ventral tubercle (Lambert et al., 2009); the absence of ventral excavations in the axis of the latter further indicates reduced insertions for the M. longus colli as compared to *M. gregarius* and *N. platyrostris*. Furthermore, the lower transverse process of C6 in the holotype of *N. urbinai* is as long transversely as the process of other posterior cervicals, thus indicating a reduced origin area for the M. longus colli. Osteological markers for insertion areas of the M. longus colli into the atlas and the axis were generally more reduced in the observed extant ziphiids as compared to *M. gregarius* and *N. platyrostris* (Table 2); the axis consistently lacks deep ventral excavations for the M. longus colli in contrast to *M. gregarius* and *N. platyrostris* (Fig. 8).

A ventral tubercle is rarely present on the atlas of extant ziphiids, except in *Mesoplodon grayi* and *Berardius* spp. (Dataset 1, Ramassamy et al., 2018). In addition, the lower transverse process of C6 is more developed in *Mesoplodon bidens*, *M. densirostris*, and *M. grayi* than in *N. platyrostris* and other crown ziphiids observed (Fig. 9d–e). This feature indicates a relatively larger origin area for the M. longus colli in these three *Mesoplodon* species.

Mm. intertransversarii ventrales cervicis. This muscle also originates from the lower transverse process of C6 (de Muizon, 1984; Schulte, 1916; Uhen, 2004). It bears multiple insertions into the posterior side of the transverse processes of the atlas, axis, C3, and C4. It participates in the lateral flexion of the neck. On the posterior side of the unfused axis of *Messapicetus gregarius* MUSM 2548, the presence of a large depression along the lower transverse process suggests a large area of insertion for the Mm. intertransversarii ventrales cervicis (Fig. 8b).

Similar insertion areas are observed in *N. platyrostris* (Fig. 8d). As for the M. longus colli, the Mm. intertransver-

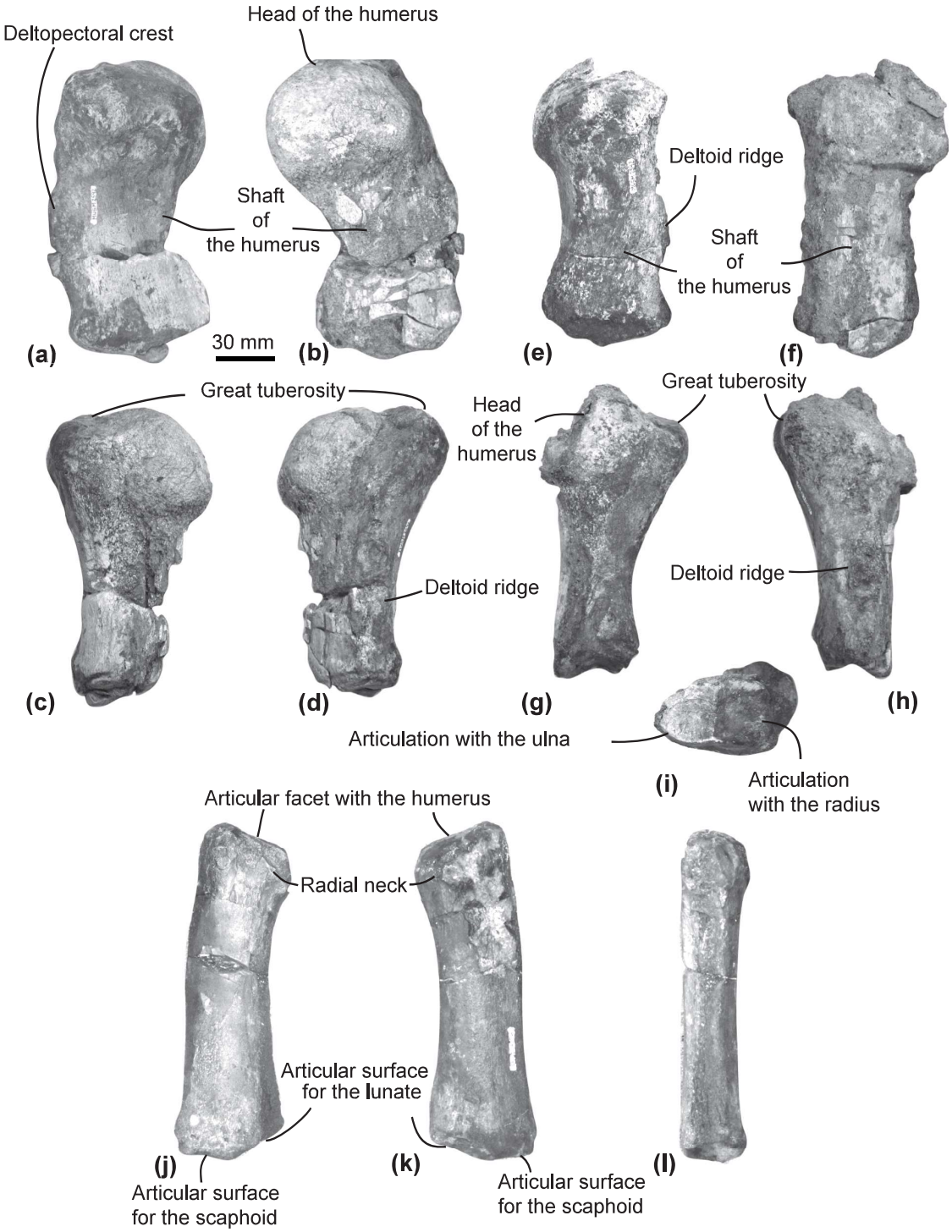

Figure 7. Humeri and left radius of MUSM 2542, *Messapicetus gregarius*. Right humerus in medial **(a)**, lateral **(b)**, ulnar **(c)**, and radial view **(d)**; left humerus in medial **(e)**, lateral **(f)**, ulnar **(g)**, radial **(h)**, and posterior view **(i)**; left radius in lateral **(j)**, medial **(k)**, and ulnar view **(l)**.

Table 2. Measurements of the vertebrae from specimen MUSM 2548, *Messapicetus gregarius*. Thoracic–post-thoracic vertebrae from A to E are ordered in relative position; e stands for estimated measurements, and "–" indicates missing measurements.

Feature	Axis	C5–C6	C7	A	B	C	D	E
Transverse width at the level of transverse processes	186e	–	–	162e	184e	–	–	–
Anterior transverse width centrum	–	73	75	69	70e	71	54e	–
anterior transverse height centrum	–	74	76	75	53	52	55	–
Posterior transverse height centrum	55	56	57	54	–	–	–	–
Posterior transverse width centrum	76	57	59	55	–	–	–	–
Anteroposterior thickness centrum	12	21	28	37	52	63	72	82
Transverse width neural canal	51	–	–	–	–	–	–	–

Table 3. Summary of the main features relative to neck musculature in extant and fossil Ziphiidae. All specimens were directly consulted.

Species	Sample	Number of fused cervical vertebrae	Ventral tubercle on the atlas	Ventral excavations on the axis	Development of the lower transverse process of C6
Messapicetus gregarius	1	0	?	present	?
Ninoziphius platyrostris	1	2	present	present	reduced
Archeoziphius microglenoideus	1	?	absent	?	?
Nazcacetus urbinai	1	2	absent	absent	reduced
Berardius sp.	2	3	present	absent	reduced
Hyperoodon ampullatus	11	7	absent	absent	absent
Mesoplodon bidens	2	3	absent	absent	more developed than in the other cervicals
Mesoplodon bowdoini	1	3	absent	absent	reduced
Mesoplodon densirostris	2	3 to 5	absent	absent	more developed than in the other cervicals
Mesoplodon grayi	1	2	present	absent	more developed than in the other cervicals
Tasmacetus shepherdi	3	5 to 6	absent	absent	reduced
Ziphius cavirostris	4	4 to 5	absent	absent	reduced

sarii ventrales cervicis likely originated from the lower transverse process of C6, even though the precise areas cannot be identified. Unlike *M. gregarius*, the atlas and axis were fused in *N. platyrostris*, considerably reducing lateral flexibility in the anterior neck region.

In *Nazcacetus urbinai* (Lambert et al., 2009), the lower transverse process of the axis is not as enlarged as in *M. gregarius* MUSM 2548, and the cervical vertebrae 3 to 7 are free, while the atlas and axis are fused.

Conversely, many extant Ziphiidae display extensive fusion of the neck vertebrae; none of the species with data available bear a free axis at the adult stage (Lambert et al., 2015). For example, in *Hyperoodon ampullatus* all cervical vertebrae are consistently fused in both males and females (Fig. 9c). With regard to the lower transverse process of C6,

as for the M. longus colli, an accurate origin of the Mm. intertransversarii cervicis could not be identified in extant ziphiids.

M. rectus capitis dorsalis major. This muscle originates from the neural spine of the axis and inserts into the nuchal crest of the supraoccipital bone (Schulte, 1916; Uhen, 2004). It extends and stabilizes the head.

Even though the neural spine of the axis is not preserved in *M. gregarius* MUSM 2548, a comparison between the stem ziphiid *N. platyrostris* and crown ziphiids is relevant. The subcomplete neural spine of the holotype of *N. platyrostris* was assessed by de Muizon (1984) to be longer and thinner than in extant ziphiids, except *Hyperoodon ampullatus* (Fig. 9). The condition of the neural spine in extant ziphiids from our dataset confirms this statement, except in the case of *Tasmacetus shepherdi*, for which the proportionally longer neural spine was closer to *N. platyrostris* than to other extant Ziphiidae. In *Nazcacetus urbinai*, the neural spine of the axis is strongly reduced compared to *N. platyrostris*, suggesting a smaller origin area for the M. rectus capitis dorsalis major.

4.2.2 Forelimb muscles

M. supraspinatus. The M. supraspinatus originates from the scapula, in the supraspinous fossa, and along the medial side of the acromion (Benke, 1993; Marx et al., 2016). It inserts into the great tuberosity of the humerus. The main action of the M. supraspinatus is to abduct the humerus.

Even though the bad preservation of the region around the supraspinatus fossa and the acromion in *M. gregarius* MUSM 2542 precludes a reconstruction of the origin of this muscle, the flattened and individualized great tuberosity of the humerus observed in MUSM 2542 suggests this muscle to be as developed as in extant Ziphiidae. Indeed, we observed an individualized great tuberosity in *Berardius* spp., *Hyperoodon* spp., *Indopacetus pacificus*, *Mesoplodon bidens*, *M. bowdoini*, *M. densirostris*, *M. grayi, Tasmacetus shepherdi*, and *Ziphius cavirostris*. A flattened great tuberosity was also present in the isolated humerus MNHN SAS 943, tentatively attributed to *Ninoziphius platyrostris* by de Muizon (1984).

M. deltoideus. The M. deltoideus originates from the infraspinous fossa, the spine of the scapula, and part of the acromion. It inserts into the lateral side of the anterior edge of the deltoid ridge of the humerus. Its main action is to extend the humerus, while the acromial fibres are involved in the abduction of the latter (Marx et al., 2016; Benke, 1993). We could not accurately assess the origin area of the M. deltoideus based on the partial scapula of *M. gregarius* MUSM 2542. Nevertheless, the presence of a deltoid ridge along the anterior surface of the humerus indicates a moderate development of this muscle as compared to Physeteroidea that display a deltoid ridge more developed proximodistally (Benke, 1993). A developed deltoid ridge is also present in MNHN SAS 943 *Ninoziphius platyrostris* and in all the extant ziphiids examined in this study.

M. infraspinatus. The M. infraspinatus originates from the posterior surface of the scapula, posterior to the M. deltoideus (Benke, 1993; Marx et al., 2016). It inserts into a small fossa distal to the head of the humerus. This muscle acts as an extensor of the humerus and slightly participates in its adduction (Benke, 1993). The posterior crest along the lateral surface of the scapula of *Messapicetus gregarius* MUSM 2542 defines posteriorly the origin of the M. infraspinatus. This crest is similarly developed as in a fragmentary scapula of MSNUP 115760 partial skeleton of *Messapicetus longirostris* described by Bianucci et al. (2016a). However, the eroded surface of the two humeri of *M. gregarius* MUSM 2542 precluded us from assessing its insertion area. In the isolated humerus MNHN SAS 943, tentatively associated with *Ninoziphius platyrostris* by de Muizon (1984), we note the presence of a fossa distal to the head of the humerus where the M. infraspinatus most likely inserted. We observe a similar fossa in *Berardius* spp., *Hyperoodon* spp., *Indopacetus pacificus*, *Mesoplodon bidens*, *M. bowdoini*, *M. densirostris*, *M. grayi, Tasmacetus shepherdi*, and *Ziphius cavirostris*.

M. teres major. The M. teres major originates from the posterior region of the scapula in the teres fossa (Benke, 1993; Marx et al., 2016). It inserts into the posteroproximal part of the humerus. This muscle adducts the humerus and allows its inward rotation. The posterior crest in the scapula of *Messapicetus gregarius* MUSM 2542, *M. longirostris* MSNUP 115670, and all extant ziphiids of the sample defines anteriorly the origin area of the M. teres major.

4.3 Statistical results

4.3.1 Hamular fossa of the pterygoid sinus

The relationship between HF proportions and deep-diving abilities was revealed as significant with and without phylogenetic correction (with phylogenetic correction: F ratio $= 12.504$; p value $= 0.001$; without phylogenetic correction: F ratio $= 18.078$; p value $= 2.82 \times 10^{-6}$). The four linear measurements taken were sufficient to distinguish ziphiid species from other odontocetes of the sample, particularly when the principal components (PCs) 1 and 2 were combined (Fig. 11). All ziphiids were characterized by an enlarged HF both anteroposteriorly and dorsoventrally as compared to other odontocetes (Fig. 11). The deep-diving species *Grampus griseus* and *Physeter macrocephalus* showed the same tendency as observed in ziphiid species. The species *Globicephala melas*, *Monodon monoceros*, and *Pseudorca crassidens* also possessed an anteroposteriorly and dorsoventrally enlarged HF, but could be distinguished from Ziphiidae based on their anteriorly wider HF. *Messapicetus gregarius* exhibited an enlarged HF similar to other Ziphiidae. However, *M. gregarius* could be differentiated from other ziphiids

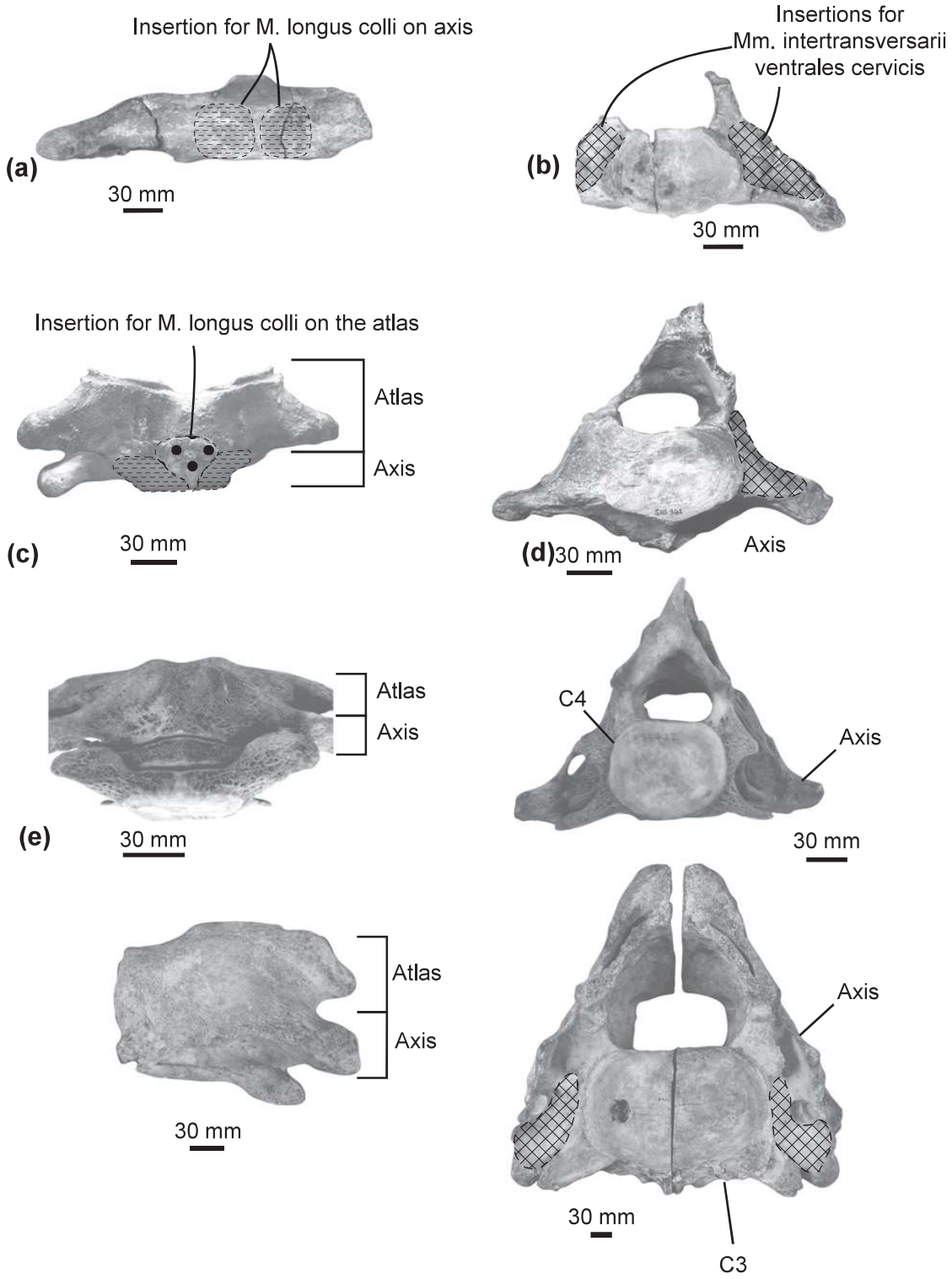

Figure 8. Comparison of muscular insertions along the atlas and axis in *Messapicetus gregarius* MUSM 2548 in ventral view **(a)** and posterior view **(b)**; in *Ninoziphius platyrostris* MNHN SAS 941 in ventral view **(c)** and posterior view **(d)**; in *Mesoplodon densirostris* USNM 593522 in ventral view **(e)** and posterior view **(f)**; in *Berardius* sp. MNHN 1885-278.

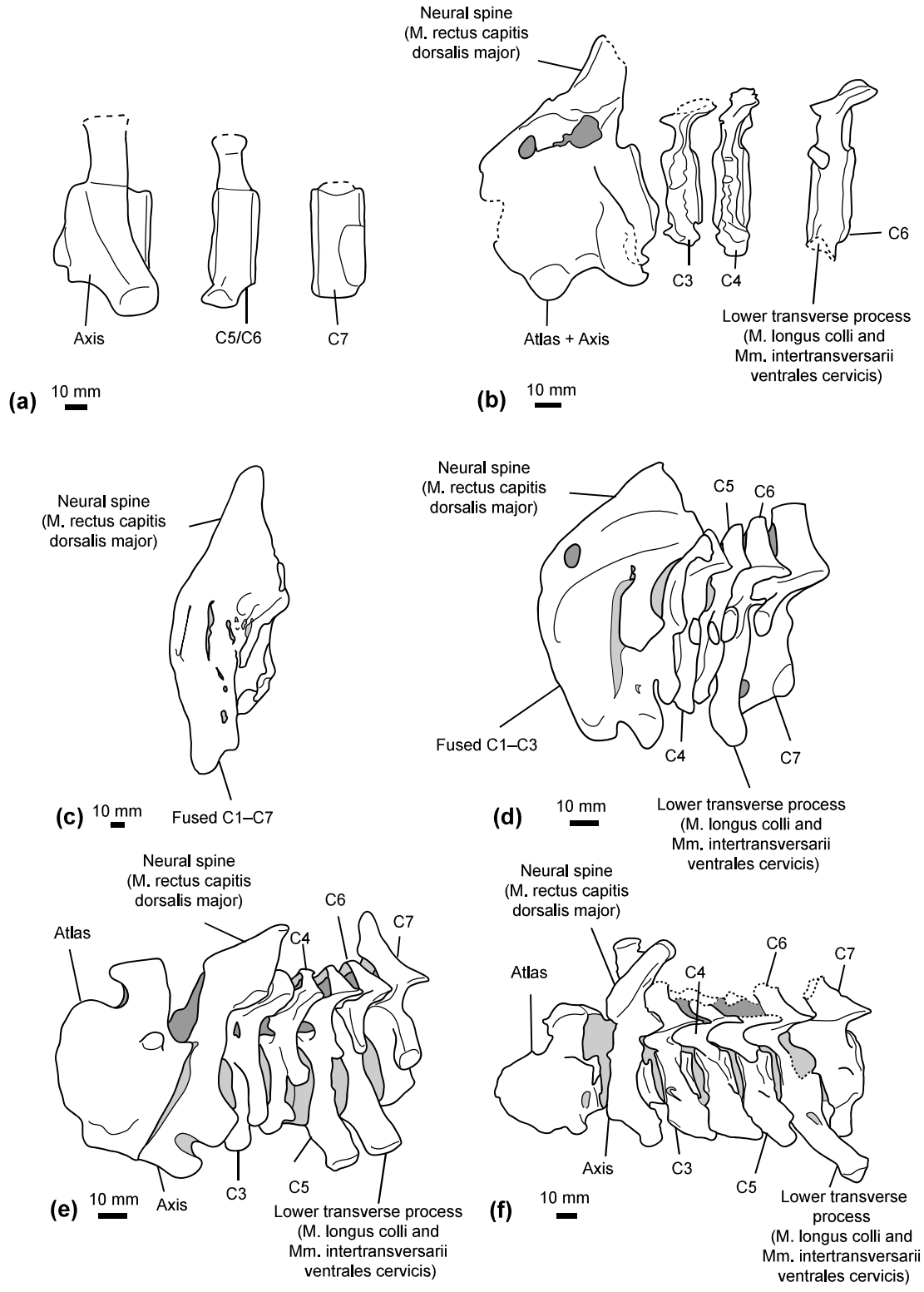

Figure 9. Comparative reconstructions of the cervical complex in several cetaceans with neck muscle origins discussed in this paper. The reconstructions concerned *Messapicetus gregarius* (MUSM 2548) **(a)**, *Ninoziphius platyrostris* (MNHN SAS 941) **(b)**, *Hyperoodon ampullatus* (SNM CN1x) **(c)**, *Mesoplodon bidens* (MNHN A14519) **(d)**, *Inia geoffrensis* (SNM CN1x) **(e)**, and *Xiphiacetus cristatus* (IRSNB 3240-M.361) **(f)**. Dotted lines correspond to broken parts.

based on its HF being posteriorly wider and dorsoventrally enlarged.

4.3.2 Forelimb

The relationship between forelimb measurements after log-shape ratio transformation and deep-diving abilities was revealed as not significant with and without phylogenetic correction (with phylogenetic correction: F ratio = 0.90638; p value = 0.5595). Ziphiidae, including *Messapicetus gregarius*, were most efficiently discriminated when PC1 (25.60 %) and PC2 (19.99 %) were combined (Fig. 12). All ziphiids exhibited a relatively elongated humerus and radius, a distally narrow humerus and radius, a shortened scapula, and a more developed deltoid tuberosity as compared to other odontocetes (Fig. 10). A similar tendency was also observed in *Physeter macrocephalus* (Fig. 12). The basilosaurid *Dorudon atrox* exhibited an even longer humerus and radius and a more developed deltoid tuberosity than extant Ziphiidae. On the other hand, the deep-diving species *Delphinapterus leucas*, *Globicephala melas, Grampus griseus*, and *Pseudorca crassidens* displayed the opposite tendency, with humerus and radius distally widened and a shortened humerus.

5 Discussion

5.1 Neck flexibility in stem Ziphiidae

Our reconstruction of neck muscles in the stem ziphiids *Messapicetus gregarius* and *Ninoziphius platyrostris* indicate a higher lateral and dorsoventral flexibility of the neck in both species as compared to other ziphiids of the sample. These stem ziphiids had extended insertion areas for the M. longus colli and the Mm. intertransversarii ventrales cervicis as compared to extant ziphiids (Fig. 9) and the late Miocene crown ziphiid *Nazcacetus urbinai*.

In addition, the proportionally longer cervical vertebrae of long-snouted stem ziphiids compared to crown beaked whales allowed for wider lateral and dorsoventral movements.

We also interpret the low degree of fusion of the cervical vertebrae in *M. gregarius* and *N. platyrostris* as an argument in favour of a more flexible neck. Even though extant cetaceans may display intraspecific variation regarding the degree of fusion of their cervical vertebrae (Buchholtz, 2001), we argue that the low degree of fusion of the cervical vertebrae in stem ziphiids is consistent for three reasons. First, we assessed the ontogenetic stages of the studied specimen of *Messapicetus gregarius* as being an adult, although the degree of fusion generally increases with age in cetaceans (Buchholtz, 2001). Second, extant ziphiids generally possess at least three fused cervical vertebrae at adult age, thus contrasting with the condition in the analysed stem ziphiids (Lambert et al., 2015). Finally, the axis of *M. gregarius* MUSM 2548 displays an anterior articular facet for the atlas, including the odontoid process. In the dog, the absence of the odontoid process results in tilting or dorsal displacement of the axis into the vertebral canal, leading to the compression of the spinal cord (Evans and Lahunta, 2013). Therefore, the presence of this articular facet in *M. gregarius* would contribute to maintaining a correct articulation between the atlas and the axis in the absence of fusion between these two elements.

The more extensive fusion of the cervical vertebrae in the extant ziphiids *Hyperoodon* spp., *Indopacetus pacificus*, *Tasmacetus shepherdi*, and *Ziphius cavirostris* likely impacted lateral movements of the neck. In those species, the lower transverse process of C6 was also reduced, indicating a reduction of the areas of origin for both M. longus colli and Mm. intertransversarii cervicis. Conversely, *M. bidens*, *M. densirostris*, and *M. grayi* possess developed C6 processes, suggesting some degree of neck flexibility among crown ziphiids.

The cervical vertebra of the specimen MUSM 2548 identified as C5–C6 bears a small lower process similar in shape and development to C6 of *N. platyrostris* (de Muizon, 1984). This condition differs from the eurhinodelphinid *Xiphiacetus cristatus*, the platanistoid *Otekaikea marplesi*, and the basilosaurid *Dorudon atrox*, in which the strong and thickened lower transverse process indicate a developed origin for the M. longus colli (Fig. 9e; Lambert, 2005; Tanaka and Fordyce, 2014; Uhen, 2004). The lack of a developed lower process in C6 may suggest a less flexible neck in *N. platyrostris* and possibly *M. gregarius* compared to the aforementioned species. Yet, both *M. gregarius* and *N. platyrostris* display large insertions for the M. longus colli and the Mm. intertransversarii ventrales cervicis that are more developed than in any extant ziphiid.

While the spinous process of the axis was not preserved for *M. gregarius*, *N. platyrostris* displays a weaker spinous process compared to other extant Ziphiidae. However, a strong spinous process is present in *Inia geoffrensis*, an odontocete with a highly flexible neck. In *H. ampullatus*, de Muizon (1984) noted a particularly strong spinous process of the axis, most likely supporting the head.

Neck rigidity might be related to deep-diving specialization in Ziphiidae. However, differences in the degree of flexibility observed among extant ziphiids advocate for a more complex functional interpretation. Data on potential differences in swimming and feeding strategies between extant ziphiid species are currently insufficient to explain the contrasted neck morphologies observed.

5.2 Forelimb morphology and its relation to deep diving

Our reconstruction of the forelimb muscles of *M. gregarius* suggest no important differences with extant ziphiids. Multivariate analyses confirm this close relation, showing that *M. gregarius* and other extant ziphiids possess a relatively